fibers

Article

Evaluation of the Maximum Strain for Different Steel-FRCM Systems in RC Beams Strengthened in Flexure

Francesco Bencardino * and Mattia Nisticò

Department of Civil Engineering, University of Calabria, Via P. Bucci Cubo 39B, 87036 Rende, Italy
* Correspondence: francesco.bencardino@unical.it; Tel.: +39-0984496923

Abstract: The strengthening of existing reinforced concrete (RC) structures by means of steel-fabric reinforced cementitious matrix (Steel-FRCM) systems has been universally recognized in the academic literature as an effective method. Several types of steel fibres can be found in the marketplace, and they are classified according to mass per unit area and tensile strength. In the flexural strengthening design of RC beams, a fundamental parameter is the effective tensile strain level in the Steel-FRCM system attained at failure. Some authors and guidelines suggest evaluating this strain value using the results of bond tests. As is well highlighted in many works, the debonding strain in Steel-FRCM composites applied on concrete beams is usually higher than that from single-lap shear tests. At this point, it can be easily obtained by applying an appropriate amplification coefficient. This study experimentally investigates the difference in the debonding strain between Steel-FRCM composites bonded to concrete blocks in single-lap shear tests (end strain) versus the debonding strain in concrete beams (intermediate strain). The results were used to critically discuss the variability of the amplification coefficient, significantly affected by the mechanical and geometrical properties of the steel fibres. Moreover, a simple predictive formula to evaluate the intermediate strain debonding was used, and the results were compared with the experimental evidence. Finally, a large database of direct shear and flexural tests was used to confirm the experimental and theoretical data obtained herein.

Keywords: steel-fabric reinforced cementitious matrix (S-FRCM); fibre/matrix bond; flexural design

Citation: Bencardino, F.; Nisticò, M. Evaluation of the Maximum Strain for Different Steel-FRCM Systems in RC Beams Strengthened in Flexure. *Fibers* **2022**, *10*, 67. https://doi.org/10.3390/fib10080067

Academic Editors: Valeria Corinaldesi and Jacopo Donnini

Received: 17 June 2022
Accepted: 2 August 2022
Published: 4 August 2022

1. Introduction

The fabric reinforced cementitious matrix (FRCM) system has become one of the most popular strengthening methods for existing reinforced concrete (RC) structures. It offers advantages compared to traditional methods: lightness, ease of installation, usability of the structure in the strengthening phases, no impact on the geometry and original structural concept, resistance to atmospheric agents, and reversibility of the intervention over time. Notably, the FRCM systems could be used in place of fibre-reinforced polymers (FRPs) systems [1].

To date, the study of new innovative materials to be used in civil engineering applications has prompted sector research to use nanocomposites. These materials have been shown to be effective in developing materials with high structural performance, as demonstrated in [2–4].

Several experimental works were carried out over the last 10 years in order to investigate the behaviour and the effectiveness of FRCM systems in the strengthening of RC structures. Fundamental information has been provided and disseminated in the scientific literature on the qualification and acceptance [5,6], tensile and bond response [7–11], and flexural and shear strengthening of full-scale RC beams [12–15].

The structural performance of RC members can also be effectively improved using steel fibre strips externally bonded by means of cementitious matrix. Many experimental investigations and analytical studies on structural members retrofitted with Steel-FRCM systems have been conducted [16–22]. In the following work, the acronym Steel-FRCM is used even if the international literature also suggests the use of the acronym Steel Reinforced Grout (SRG). Steel fibre with different mechanical and geometrical properties are available in the marketplace. Consequently, the performance of the different Steel-FRCM systems is still to be fully understood. The outgoing technical documents have not yet incorporated all the types of existing steel fibres, such as stainless or galvanized steel. The wide range of steel fibres allows the designers to choose the best option in the strengthening phase. The mechanical properties of the steel fibres considered in this paper range between 1470 ÷ 2000 MPa for tensile strength and between 600 ÷ 2200 g/m^2 for the mass per unit area.

The development of a reliable and accurate design model for the Steel-FRCM systems is the last step to fully characterizing this type of composite system. Therefore, the extensive knowledge of the structural behaviour achieved over time for these strengthening systems has been transferred into some design documents. Until now, two major international guidelines [23,24] have issued the first requirements for the definition of the debonding strain for flexural strengthening of RC members. The scientific community has focused its efforts on defining reliable design approaches in the prediction of the debonding strain of the external strengthening system. The present work attempts to address this issue on the basis of available experimental data.

The research significance is to investigate the variability of a transition coefficient for the Steel-FRCM composite in the flexural strengthening of RC beams. As a result, the community may be encouraged to improve the design provisions.

The experimental results highlighted that the failure of the RC strengthened member mainly occurs due to the loss of bond between the composite system and the concrete substrate. Specifically, the external additional action loses effectiveness at the debonding of the composite system. Combining the results of single-lap shear tests with tensile tests on dry fibre strips, it is possible to evaluate the design parameters for externally bonded Steel-FRCM systems in flexure (intermediate debonding strain), according to [24]. The goal is to evaluate the effective relationship between the strain that correspond to the flexural failure in RC beams and the strain due to the detachment in bond tests.

In order to determine the effectiveness of this design approach, two different steel fibres, characterized by high and low mass per unit area, were used in combination with the same cementitious matrix. In one case, the matrix allowed the tensile failure of the fibre in both single-lap and flexural tests to be achieved. Instead, using the high mass per unit area steel fibre, low level of strain is achieved in the bond test while the performance significantly increases in terms of debonding strain in flexure.

Therefore, the procedure shows that the results, expressed through the amplification coefficient, are strongly influenced by the geometrical and mechanical properties of the different reinforcing steel strips. Based on those results, further considerations on the assessment of the coefficient α must be addressed in order to define the transition between end and intermediate strain.

Then, the analytical formula defined in Bencardino et al. [25] was used to estimate the intermediate debonding strain obtaining reliable results. The main aim of the article is to assess the accuracy of both methods (guideline procedure and predictive formula) against an experimental database collected from the literature obtaining useful information regarding the design of these materials.

2. Material Properties: Steel Fibres, Concrete, and Cementitious Matrix

The experimental programme included both a development phase and an execution phase. The development phase concerned a series of physical operations to prepare 24 samples: specifically, 18 specimens for single-lap shear tests and 6 specimens for direct tensile tests. The execution phase of this programme concerned the experimental tests and analysis of the results.

2.1. Steel Fibres

Two different unidirectional steel fibres were used, Stainless Steel (SS) [26] and Galvanized High Strength Steel (GLV) [27]. The acronym SS indicates a unidirectional strip made with stainless steel (AISI 316) strands, particularly resistant to corrosion, which can be used in the interventions on surfaces subject to rising damp and, in general, exposed to aggressive environments. Each strand is composed of seven wires and, in turn, made up of seven other threads twisted around each other. It is an austenitic (non-magnetic) stainless steel alloy composed of a low carbon content (~0.05%). The GLV is a unidirectional reinforcement made of five high strength galvanized zinc plated filaments rolled up longitudinally. Figure 1a,b show the steel strips 50 mm wide (b_f) and the single steel strand for SS and GLV, respectively.

(**a**) (**b**)

Figure 1. Steel strips and detail of a single strand: (**a**) SS; (**b**) GLV.

The number of strands (n_{str}) in a 50 mm strip width, the actual area of a single steel strand ($A_{f,str}$), the cross-section area of the steel strip (A_f), and the nominal thickness (t_f) and the mass per unit of area (ρ) of the two types of unidirectional steel strips, SS and GLV, are given in Table 1.

Table 1. Geometrical properties of the dry fibres and strips.

Description	Label	$A_{f,str}$ (mm^2)	n_{str}/50 mm	A_f (mm^2)	t_f (mm)	ρ (g/m^2)
Stainless Steel	SS	0.470	25	11.75	0.235	2200
Galvanized High Strength Steel	GLV	0.519	8	4.15	0.083	650

2.2. Cementitious Matrix

The SS and GLV steel fibres were applied using an inorganic cementitious matrix (BMN) [28]. The BMN is a non-shrink, normal curing, ready-to-use, thixotropic mortar with the addition of synthetic short fibres. It has high mechanical strength for both short and long curing time, strong adhesion to concrete, high resistance against sulphates, and excellent durability even in severe aggressive conditions (coastal areas, de-icing salts, acid rain). The matrix was certified according to EN 1504-3:2005 [29] and EN 1504-4:2004 [30] specifications concerning the structural requirements.

The compressive (f_m) and tensile (f_t) strength of the cementitious matrix were obtained by using prismatic specimens of dimensions 160 mm × 40 mm × 40 mm (Figure 2a). Specifically, five samples were used for flexural tests and ten samples for compression tests. A mechanical machine with 100 kN capacity was used and the tests were carried out according to EN 12190:1998 [31] for the compressive strength and to EN 1015-11:2019 [32] for the flexural tensile strength. Figure 2b,c show the flexural and compression test of the matrix, respectively.

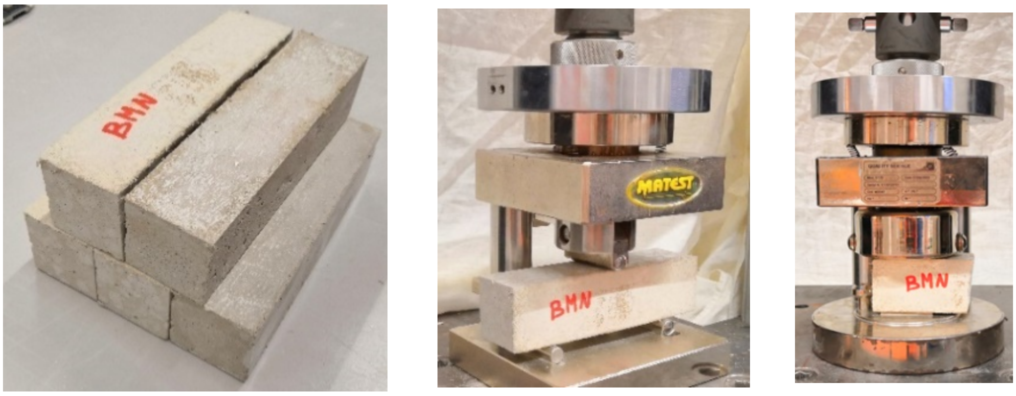

(**a**) (**b**) (**c**)

Figure 2. Cementitious matrix: (**a**) prismatic samples; (**b**) flexural test; (**c**) compression test.

2.3. Concrete

Cylindrical compressive strength (f_{cm}) and tensile splitting strength (f_{ctm}) of the concrete used to prepare the prisms for the subsequent single-lap shear test were evaluated using three samples of 150 mm diameter (D) × 300 mm height (H) (Figure 3a). Figure 3b,c show the compression and splitting test on concrete, respectively. The experimental mean values for the cementitious matrix and concrete are given in Table 2.

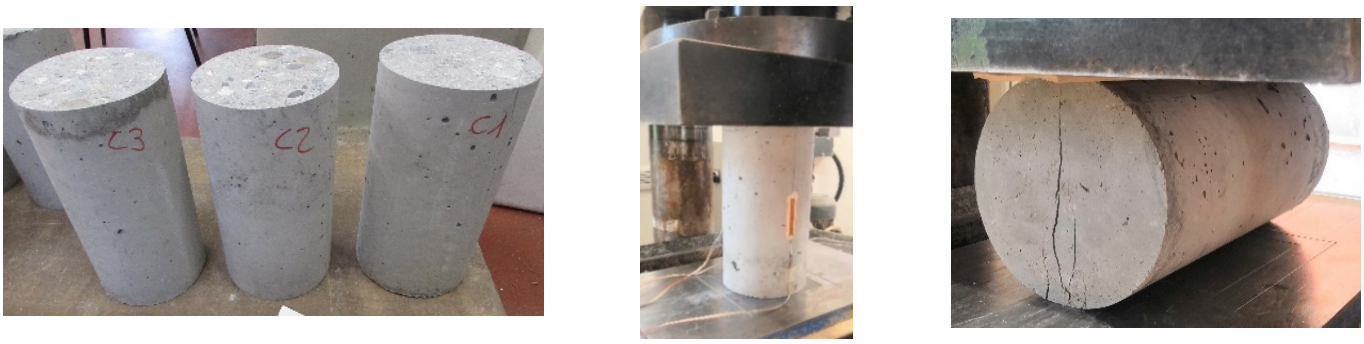

(**a**) (**b**) (**c**)

Figure 3. Concrete: (**a**) cylindrical samples; (**b**) compression test; (**c**) splitting test.

Table 2. Mechanical properties of the cementitious matrix and concrete.

Property	Mean Value (N/mm^2)	
	Cementitious Matrix	Concrete
Compressive Strength f_m, f_{cm}	43.67	33.89
Tensile Strength f_t, f_{ctm}	5.77	2.87

Concrete prisms were formed using wooden formworks. Two different geometrical configurations were used: 150 mm (b_c) × 150 mm (p_c) × 400 mm (l_c) according to the suggestion given in [24] and 200 mm (b_c) × 200 mm (p_c) × 320 mm (l_c), respectively. The surfaces where the Steel-FRCM system was bonded were slightly roughened by mechanical brushing and a series of notches were made in order to increase the adhesion capacity (Figure 4a,b). All the specimens were cast in a laboratory and cured in standard environmental conditions.

(**a**) (**b**)

Figure 4. Surface roughness of the two geometrical configurations: (**a**) prism with 150 mm × 150 mm × 400 mm dimensions; (**b**) prism with 200 mm × 200 mm × 320 mm dimensions.

2.4. Direct Tensile Test: Test Set-Up and Results

In order to define the mechanical properties of the strengthening systems, three specimens of each type of steel strip were subjected to direct tensile tests. All strips were 50 mm wide (b_f = 50 mm) and 500 mm long. The specimens were identified according to the notation DT_x_y, where DT is the acronym of Direct Tensile, x identifies the type of steel fibre, and y is the progressive number of the specimen (Table 3). Rectangular aluminium tabs of 3 mm in thickness, 100 mm in length, and 50 mm in width were glued at both ends, employing a thin layer of suitable epoxy resin with high compressive strength (76 MPa). The tensile tests were carried out with a displacement controlled tensile machine Zwick-Roell Z250 with a load capacity of 250 kN using a rate of 0.5 mm/min.

Table 3. Direct tensile test results of the dry fibre SS and GLV specimens.

Specimen	F_{max} (N)	f_f (N/mm^2)
DT_SS_1	16,618.75	1414.36
DT_SS_2	15,664.90	1333.18
DT_SS_3	18,142.54	1544.05
Average	16,808.73	1430.53
(C.o.V.)	(0.074)	(0.074)
DT_GLV_1	8507.78	2050.07
DT_GLV_2	8318.67	2004.50
DT_GLV_3	7924.88	1909.61
Average	8250.44	1988.06
(C.o.V.)	(0.036)	(0.036)

The Figure 5 shows the direct tensile test on SS (Figure 5a) and GLV (Figure 5b) strips while Figure 6 shows the stress–strain curves obtained for both dry fibres, SS (Figure 6a) and GLV (Figure 6b), respectively.

The stress–strain curves (Figure 6) show an initial elastic linear behaviour followed by a non-linear stage due to the progressive rupture of the single wires of the strands until to the peak load, then the curves drop at failure.

(**a**) (**b**)

Figure 5. Direct tensile test on dry fibres: (**a**) SS strip; (**b**) GLV strip.

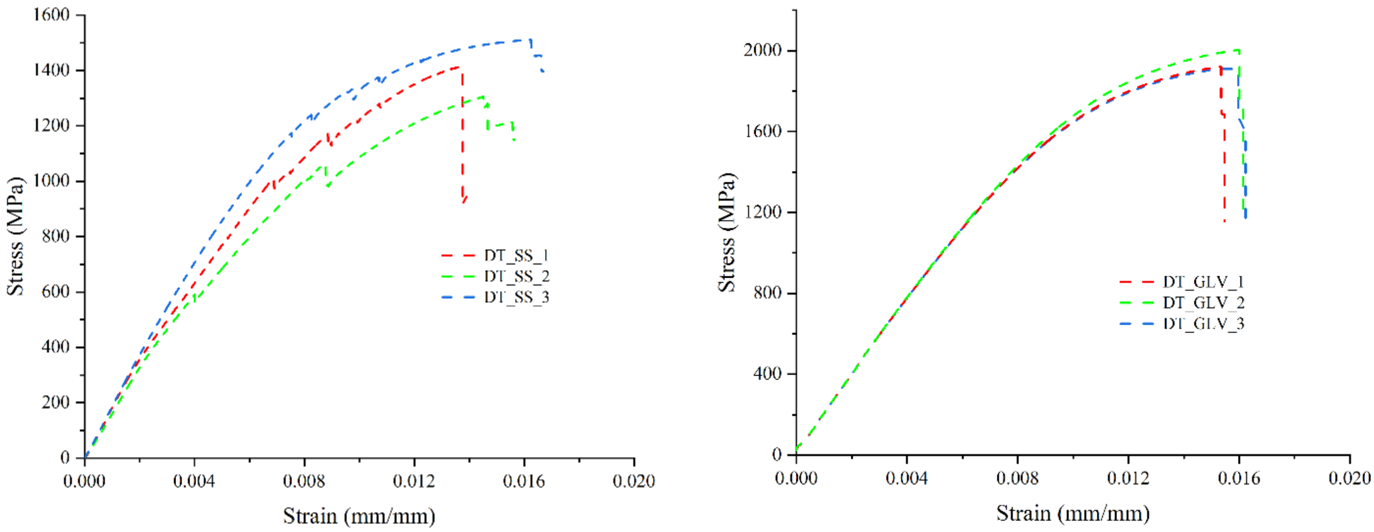

(**a**) (**b**)

Figure 6. Stress–strain curves of the direct tensile tests on dry fibres: (**a**) SS strip; (**b**) GLV strip.

The values of the maximum load (F_{max}) and tensile strength (f_f) of each SS and GLV specimen were given in Table 3. In the same Table 3, the average values and the coefficient of variation (C.o.V.) for each set of specimens are given.

With reference to the average values, the tensile strength was 1988.06 N/mm^2 for GLV fibres and 1430.53 N/mm^2 for SS fibres. The GLV fibre shows a tensile strength 39% higher than SS fibre. The elastic modulus (E_f) of the SS fibres was evaluated with reference to a tensile strain level of 0.003, within to the linear stage. The values were 206,794 MPa and 198,352 MPa for SS and GLV strips, respectively. The results obtained are very similar to those provided in the manufacturer datasheets [26,27]. All the subsequent calculations were carried out with reference to 206 GPa for both types of steel fibres, SS and GLV.

3. Bond Behaviour

3.1. Direct Single-Lap Shear Test: Preparation and Test Set-Up

To study the bond performance, the classical direct single-lap shear test was used. The width of the Steel-FRCM system was b_f = 50 mm for all specimens. Some studies investigated the effective bond length (l_b) of Steel-FRCM on concrete surfaces providing useful recommendations [33,34]. The steel strips were bonded to the centre of each prism face with a bond length l_b = 260 mm. Specifically, the same bond length and width were adopted for all specimens. Table 4 summarizes the geometrical configuration of all tested concrete specimens.

Table 4. Geometric configuration of all tested concrete specimens.

Specimen ID	b_c (mm)	p_c (mm)	l_c (mm)	b_f (mm)
1 to 4	150	150	400	50
5 to 9	200	200	320	

An un-bonded length of 30 mm was left from the upper edge of the prisms to the Steel-FRCM composite system. This configuration prevents the fracture of the corner prism in the debonding process.

Figure 7 shows the bonding procedure of the Steel-FRCM system on concrete prisms. Specifically, the laboratory work was carried out according to the following steps: cleaning of the concrete surface of dust and other elements (Figure 7a,b), spreading and application of the first layer of matrix by 5 mm thick wooden forms (Figure 7c), application of unidirectional steel strip, and application of the second layer of matrix to complete the Steel-FRCM system (Figure 7d). In order to forestall any air pockets in the impregnation process, the matrix was manually pounded with a putty knife.

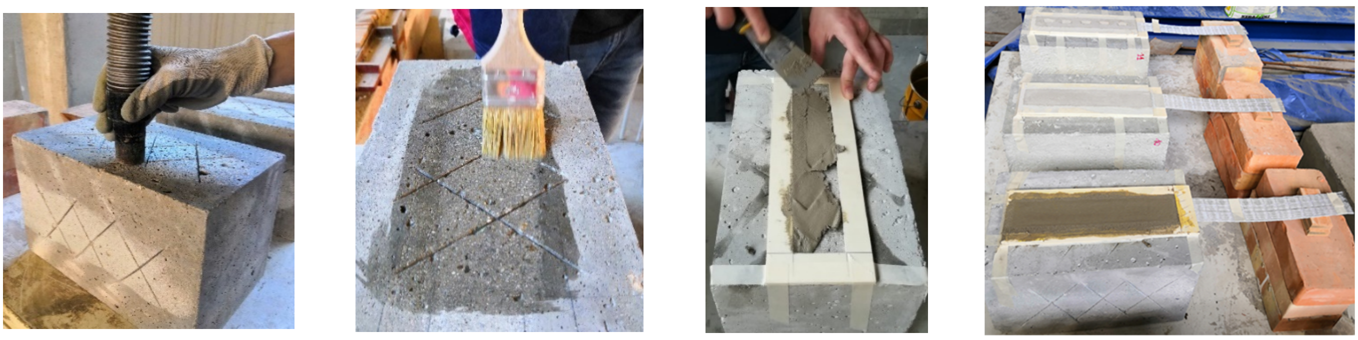

(**a**) (**b**) (**c**) (**d**)

Figure 7. Bonding procedure of the S-FRCM system on concrete prism: (**a**) cleaning procedure, (**b**) wetting of the surface, (**c**) spreading and application of the matrix layer, (**d**) final results.

Each specimen was labelled with the notation DSC_x_y, where DSC indicates the words Direct Shear Concrete, x identifies the steel fibre used (SS or GLV), and y shows the progressive number of the specimens. A total number of 22 samples were prepared, 11 samples with SS fibres and 11 samples with GLV fibres. Test set-up configuration and geometrical dimensions are given in Figure 8.

The experimental studies available in the literature show that different testing procedures have been used and highlight that the results are strongly influenced by the test set-up parameters [35–37]. Therefore, the failure mode is affected by the testing procedure. The tests were carried out according to the well-known push-pull scheme suggested by RILEM TC-250 recommendations [38]. The samples were vertically oriented and located inside a rigid steel frame able to prevent displacements and rotations. When the load was applied, the steel plate pushes the prism, and the steel strip was pulled, inducing tensile stress in the Steel-FRCM strengthening system until failure occurs. A universal INSTRON 5582 machine with a loading cell of 100 kN was used to carry out the experimental investigation. The tests were conducted under displacement control at a velocity rate of 0.2 mm/min, until failure. The specimens were aligned within the testing machine to reduce accidental eccentricities during the test, ensuring the alignment of the load plane and the Steel-FRCM strengthening system. The relative displacement between steel strip and substrate (global slip) was recorded by means of two Linear Variable Displacement Transducers (LVDTs) with a measuring range of 20 mm. A thin L-shaped aluminium plate was glued onto the dry fibres near the unbonded part of the strip and used as reference point for the measurement of slip during the test. Two rectangular aluminium tabs were applied at the end of the bare steel strip using epoxy resin. Finally, the load was applied clamping the tabs in the gripping system of the machine.

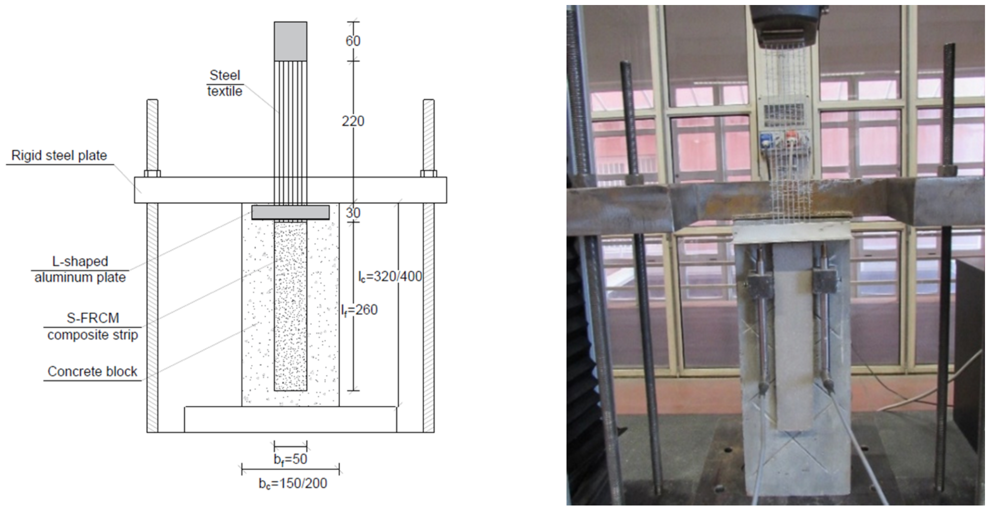

(**a**) (**b**)

Figure 8. Experimental set-up for single-lap shear test: (**a**) geometrical dimensions; (**b**) DSC_GLV_1 sample in the testing machine.

3.2. Direct Single-Lap Shear Tests: Results

Table 5 shows the main results: specifically, the maximum load in each test (P_{max}), average global slip at maximum load (g_{max}), and average ultimate global slip (g_u), both measured by the two LVDTs, maximum stress in the steel strip (σ_{max}), ratio between maximum stress in the steel strip and the tensile strength of the dry fibres (σ_{max}/f_f), the failure mode. The maximum stress in the steel strip was obtained by dividing the recorded maximum load by its cross-section area ($\sigma_{max} = P_{max}/A_f$).

For GLV system, the global slip at maximum load corresponds to the global slip at failure because the fibres reach the rupture without debonding (failure mode E). The load-global slip curves for the SS and GLV tested specimens are given in Figure 9.

The two Steel-FRCM systems show different behaviour. For the SS system (Figure 9a), the curves are characterized by an initial linear elastic branch up to about 70% of the peak load (maximum load reached). Exceeding this load, visible cracks occur in the upper layer of the matrix, the slope of the curve decreases, and the degradation of the bond strength starts (internal micro-damage).

Later, the load remains almost constant, and the curves were characterized by sudden falls (drops), owing to the increasing cracking of the external layer of the matrix. In the last stage, a gradually debonding failure took place up to a complete or partial detachment of the Steel-FRCM system from concrete surface of the prism, a very brittle debonding evolution and a sudden decay of the load up to zero was recorded.

Table 5. Experimental results of the direct single-lap shear tests.

Specimen	P_{max} (kN)	g_{max} (mm)	g_u (mm)	σ_{max} (MPa)	σ_{max}/f_f (%)	Failure Mode
DSC_SS_1	5.36	0.34	0.57	456.17	31.89	B-C
DSC_SS_2	5.71	0.59	0.65	485.96	33.97	B
DSC_SS_3	5.24	0.57	0.65	445.96	31.17	B-C
DSC_SS_4	5.98	0.79	0.81	508.94	35.58	B-C
DSC_SS_5	6.70	0.66	0.85	570.21	39.86	B-C
DSC_SS_6	5.16	0.61	0.64	439.15	30.70	B-C
DSC_SS_7	5.93	0.54	0.77	504.68	35.28	B-C
DSC_SS_8	5.65	0.65	0.77	480.85	33.61	B
DSC_SS_9	5.97	0.68	0.68	508.09	35.52	B
Average (C.o.V.)	5.74 (0.083)	0.60 (0.204)	0.71 (0.131)	488.89 (0.083)	34.18 (0.083)	
DSC_GLV_1	6.99	0.94	0.94	1684.34	85.34	E
DSC_GLV_2	7.67	1.06	1.06	1848.19	93.65	E
DSC_GLV_3	7.44	1.63	1.63	1792.77	90.84	E
DSC_GLV_4	7.62	0.80	0.80	1836.08	93.03	E
DSC_GLV_5	8.19	1.05	1.05	1973.53	100.00	E
DSC_GLV_6	8.58	0.88	0.88	2067.82	104.77	E
DSC_GLV_7	7.02	0.89	0.89	1691.74	85.72	E
DSC_GLV_8	7.80	1.02	1.02	1880.57	95.29	E
DSC_GLV_9	7.78	1.12	1.12	1874.37	94.97	E
Average (C.o.V.)	7.47 (0.068)	0.93 (0.260)	0.93 (0.260)	1849.93 (0.066)	93.73 (0.066)	

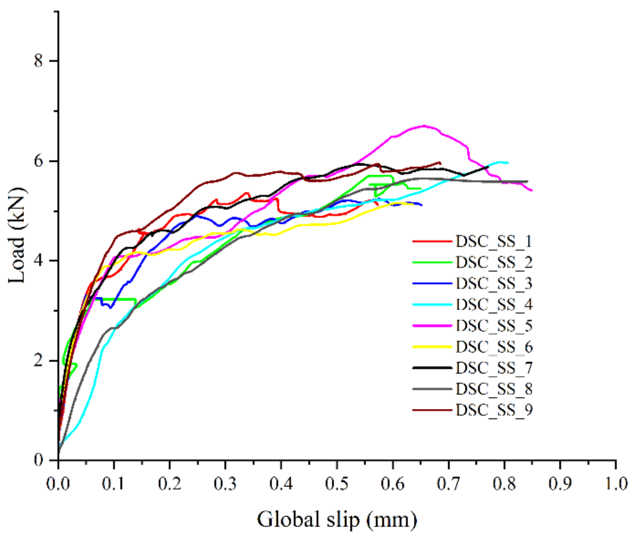

(**a**)

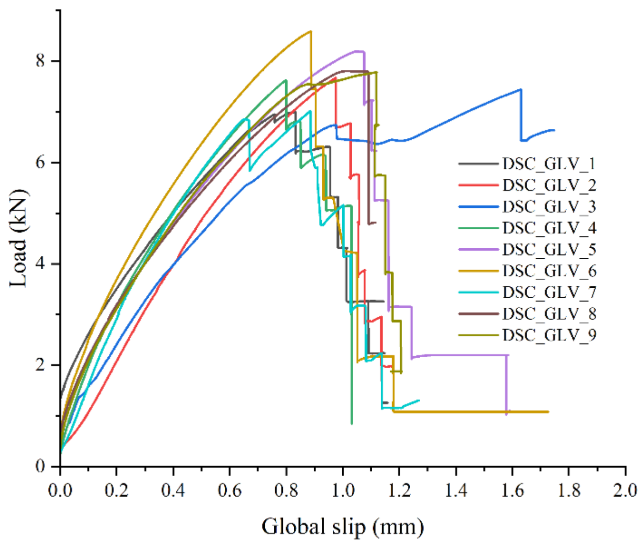

(**b**)

Figure 9. Experimental results of direct single-lap shear tests: (**a**) SS system; (**b**) GLV system.

The experimental findings highlighted that the bond behaviour is largely affected by the strand spacing in the width of the steel strips.

With reference to GLV system, the tests show the rupture of the steel strands out of the bonded area with exploitation of the total strength of the steel fibres without debonding failure. This system shows an almost linear behaviour up to the rupture of the steel fibres. The ultimate loads of the SS systems (Figure 9a) were lower than the GLV systems (Figure 9b).

Therefore, the recorded stresses at failure state of the DSC_SS system reveal a considerable decrease (of 74.12%) compared to the DSC_GLV system. In terms of global slip between composite material and concrete surface, the results suggested an increasing of about 23.65% when the galvanized (GLV) steel is applied on the specimens with respect to Stainless steel (SS), using the same cementitious matrix (0.93 mm and 0.71 mm, respectively). The results suggest that the different roughness of the surface does not affect the behaviour as can be seen from the load—slip relationship and the failure modes (Figure 10a,b).

(**a**) (**b**) (**c**)

Figure 10. Typical failure modes obtained: (**a**) SS (failure B-C); (**b**) SS (failure C); (**c**) GLV (failure E).

Even the failure modes of concrete specimens are observed and recorded in detail. In the DSC_SS system, the typical failure modes are debonding at the matrix-to-substrate interface (mode "B") and debonding at the textile-to-matrix interface (mode "C"). These two failures were identified separately on some specimens and in combined in others (Table 5). As regards the DSC_GLV system, failure occurred in all specimens due to the rupture of the galvanized steel fibre (mode "E") before any debonding could occur and consequently without affecting the matrix layer of the Steel-FRCM composite. In all the tests, the failure mode does not involve the concrete surface (Figure 10c). It will be shown later that the different bond behaviour has a significant influence on the flexural design.

4. Theoretical Calculations and Predictive Formula for Flexural Design

4.1. End Debonding Strain Value

The failure occurred in fibric-reinforced composites implicate complex interactions with stress transfer that could interest many interfaces. The most prevalent failure involves the matrix–fibre interface (at the internal or external layer) or concrete substrate-matrix interface. Rarely it engages the detachment of the concrete substrate. The debonding modes described above are typically observed in Steel-FRCM systems. Despite the difficulty in the prediction of the behaviour of FRCM-strengthened RC elements, a simplified procedure can be used due to set the debonding strain occurred in full-scale RC beam tests.

A Guideline for the design and construction of strengthening interventions with FRCM systems was issued by the Italian National Research Council (CNR) by means of the CNR-DT 215/2018 [24] document. The guideline aims to provide non-binding recommendations for designers aiming to use cement-based reinforcement systems in the field of rehabilitation of existing structures. Based on that, this document supplied specific design rules for each structural application of FRCM systems.

The goal is to investigate the reliability of this design approach in the definition of the debonding strain in flexural application of Steel-FRCM/concrete strengthening systems.

From the load–global slip curves, shown in Figure 11a,b, it is possible to identify the end strain value ($\varepsilon_{lim,conv}$) by means of the intersection between the straight line corresponding to the stress peak value ($\sigma_{lim,conv} = P_{max}/A_f$), which was determined by shear bond tests, and the stress–strain relationship of the tensile tests carried out on dry steel strips. The Figure 11 shows the procedure considering the average values.

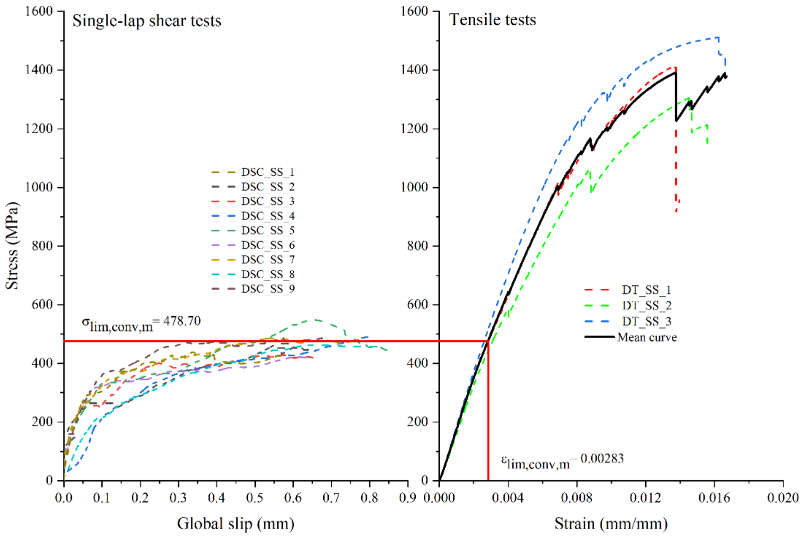

(**a**)

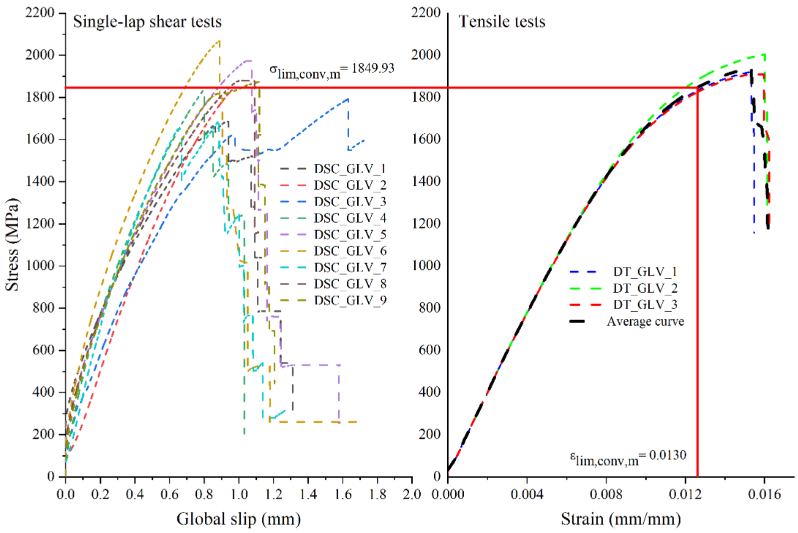

(**b**)

Figure 11. Evaluation of end debonding strain value for: (**a**) SS system; (**b**) GLV system.

For the SS system, the calculation can be made automatically. Low values of the shear bond test (input data) fall within the linear elastic phase of the curve that characterizes the tensile strength of the steel fibre. When the stress is high (as in the case of GLV system), it intersects the non-linear part of the curve and the procedure of dividing the stress by the elastic modulus would lead to an error in the calculation of the strain.

Specifically, each value of the shear bond stress was combined with the mean curve of the dry fibres in order to obtain the mean and characteristic (defined as conventional) values for the end debonding strain ($\varepsilon_{lim,conv}$) and the intermediate debonding strain ($\varepsilon^{(\alpha)}{}_{lim,conv}$). The latter is obtained by multiplying the $\varepsilon_{lim,conv}$ by the α = 1.5 factor, as suggested in the CNR guideline. The characteristic (5% fractile) value $\varepsilon_{lim,conv,k}$, required by the guidelines, is calculated as the mean value $\varepsilon_{lim,conv,m}$ minus the coefficient k_n multiplied by the standard deviation s_x. k_n is a coefficient that depends on the number of tested specimens, as reported in Eurocode 0 for unknown values [39]. The calculation was carried out by organizing the experimental results first, according to the size of the concrete blocks b_c and the width of the reinforcement strip b_f. Then, the procedure was repeated using all the available results. The qualification parameters (characteristic values) for the two Steel-FRCM systems were listed in Table 6. The same table shows the values of the standard deviations s_x, the coefficients of variation C.o.V., the coefficient k_n, the characteristic end strain $\varepsilon_{lim,conv,k}$, and characteristic intermediate strain $\varepsilon^{(\alpha)}{}_{lim,conv,k}$. For the SS system, the first group was constituted of the specimens DSC_SS_1, DSC_SS_2, DSC_SS_3, and DSC_SS_4. The second group, instead, of the remain specimens (5, 6, 7, 8, and 9). For GLV systems, the first group was assembled with specimens DSC_GLV_1, DSC_GLV_2, DSC_GLV_3, whereas the second with the results of specimens 4,5, 6, 7, 8, and 9. Finally, the procedure was repeated for all the 9 specimens tested. Therefore, the values of the coefficients k_n corresponding to 3, 4, 5, 6, and 9 samples, are 3.37, 2.63, 2.33, and 1.96, respectively.

Table 6. Statistical data evaluated combining each value of single lap-shear tests with tensile results of dry fibre.

System	N° of Specimens	b_c (mm)	$\sigma_{lim,conv,m}$ (MPa)	$\varepsilon_{lim,conv,m}$	s_x	C.o.V. (%)	k_n	$\varepsilon_{lim,conv,k}$	$\varepsilon^{(\alpha)}{}_{lim,conv,k}$	α_{real}
SS	4	150	474.26	0.00274	0.00019	7.02	2.63	0.00223	0.00335	2.16
	5	200	500.60	0.00292	0.00032	11.03	2.33	0.00217	0.00325	2.03
	9	150/200	488.89	0.00284	0.00027	9.60	1.96	0.00230	0.00346	2.09
GLV	3	150	1775.10	0.0117	0.00129	10.98	3.37	0.00738	0.0111	1.31
	6	200	1887.35	0.0135	0.00183	13.50	2.18	0.00954	0.0143	1.13
	9	150/200	1849.93	0.0129	0.00182	14.08	1.96	0.00936	0.0140	1.18

As results, the characteristic end debonding strain ranged between 0.00217 to 0.00230, and the corresponding characteristic intermediate strain was between 0.00325 and 0.00346 for the SS system. The values obtained for the GLV system range from 0.00738 to 0.00954 (characteristic end strains) and from 0.0111 to 0.0143 (characteristic intermediate strains), respectively. As can be seen from the coefficients of variation, the average values differ little from the characteristic values and, furthermore, the width of the concrete prisms does not affect the final results. Indeed, as expected, the values of strain attained by the galvanized Steel-FRCM system (GLV) is higher than the stainless Steel-FRCM system (SS) thanks to the lower spacing between cords, as suggested by the efficiency ratio. From here on, the results obtained from all 9 samples of both Steel-FRCM systems will be used.

The characteristic intermediate strain must be divided by the partial factor in order to obtain the design value. According to the document, the partial factor is equal to 1.5 for Ultimate Limit State. It should be noted that the amplification coefficient and the safety factor, both equal to 1.5, would cancel each other out. The procedure would lead to design of the strengthening system with the characteristic end strain, affecting the flexural strength of the Steel-FRCM-strengthened beams.

4.2. Predictive Formula for Intermediate Debonding Strain

Simple predictive formula has been proposed for the flexural debonding strain in Steel-FRCM strengthening applications [25]. Equation (1) shows that the strain is related to the axial stiffness of the reinforcement ($E_f t_f n_f$). The coefficients 2.24 and 0.52 consider the elastic/fracture properties of the fibre–matrix interface and other uncertainties. Specifically, they take into account the several cementitious matrices and fibres properties. However, as demonstrated in [40], by expanding the database, the coefficients can assume a different value but, at the same time, by considering the highest and lowest values of the coefficients, the relationships provide close results. Table 7 shows the results obtained, where $\varepsilon_{f,deb}$ represent the intermediate debonding strain evaluated using the predictive formula.

$$\varepsilon_{f,deb} = 2.24 \cdot (n_f E_f t_f)^{-0.52} \tag{1}$$

Table 7. Intermediate debonding strain calculated by means predictive formula.

Strengthening System	$\varepsilon_{f,deb}$
SS	0.00821
GLV	0.0141

5. Theoretical–Experimental Comparison and Analysis

The comparison in terms of flexural debonding strain was made, for the SS fibre, using flexural tests available in [41], where the experimental failure strains ($\varepsilon_{f,exp}$) were experimentally measured by linear SGs on two tested beams, with a benchmark of 0.00599 and 0.00587 (0.00593 is the average value). For the GLV system, the failure is governed by the tensile strength of the textile rather than by the debonding of the Steel-FRCM system. Therefore, the design strain of this system was directly compared with the ultimate strain of the dry textile due to the failure mode, resulting from the direct shear tests (0.0153). In addition, the last column of Table 6 reports the comparison between the intermediate strain ($\varepsilon_{f,exp}$) obtained experimentally and the end strain ($\varepsilon_{lim,conv,m}$) given as ratio (α_{real}).

An evaluation of the debonding strain was also specified in the ACI 549.4R-20 American Guideline [23]. According to this document, the value of strain attained at failure in the FRCM reinforcement ε_{fe} should be limited to the design tensile strain of the FRCM composite material ε_{fd}, and it is defined as $\varepsilon_{fe} = \varepsilon_{fd} \leq 0.012$. This approach takes into account the mechanical properties of the FRCM materials and neglects the bond behaviour.

It can be concluded that the CNR-DT 215/2018 Guideline leads to extremely low intermediate strains for the high-density fibre (SS), compared with the experimental debonding strain values. The value of α_{real} is around 2: higher than the coefficient 1.5. On the other hand, the predictive formula provides a slightly higher value than the experimental reference, which can be easily corrected with a suitable safety factor (γf = 1.2 ÷ 1.5) that should be used when debonding failure occurs. For the GLV system, the two methods provide the following results: the coefficient proposed by the Guideline is higher than that obtained from the experimental results (α_{real} equal to 1.2), while the predictive formula provides reliable value. It is worth noting that the failure mode of the GLV system occurs without debonding (fibre rupture in both bond and flexural tests) and α coefficient is equal to 1.

The same procedure was repeated using a database of experimental results collected to assess the design strain. Experimental tests carried out on RC beams externally reinforced in flexure [21,41–43] (Table 8) and single-lap shear tests [44–47] (Table 9) with Steel-FRCM composite systems were found in the scientific literature.

The properties of the steel textile declared by the authors were reported in Table 10, where all acronyms were presented in the previous sections. With E_{f1} is indicated the elastic modulus of the external reinforcement obtained from the technical data sheet and with E_{f2} from the experimental tests. In the calculation, the nominal thickness of the fibres and Young's modulus of the fibre are provided by the manufacturer or identified in the published papers. The data examined were divided according to the textile density: low (L), medium (M), and high (H). Specifically, the following data are reported in Table 8: beam width (b_c), beam height (H), effective height (h), effective length between supports (l), shear span length (a), average compressive strength of the concrete (f_{cm}), yield strength of the internal steel bars (f_{ym}), the transversal area of the steel bars in tension (A_s), the area of external reinforcement referred to the dry textile (A_f), and the experimental value of the intermediate debonding strain ($\varepsilon_{f,max}$).

Table 8. Experimental database of flexural tests of RC members strengthened with S-FRCM composites.

Experimental Work	ID	b_c (mm) H (mm) h (mm)	l (mm) a (mm) b_f (mm)	f_{cm} (N/mm^2) f_{ym} (N/mm^2) ρ_f	A_s (mm^2) A'_s (mm^2)	Reinforcement	$\varepsilon_{f,max}$
Barton et al. [42]	SRG-2	203 305 2438	2134 711.50 152	36.50 436.00	396.90 141.70	Hardwire 3SX	0.0065
Napoli and Realfonzo [21]	SRG-1LD SRG-2LD SRG-1MD SRG-1MD-A SRG-1MD-B SRG-2MD	400 200 167	3400 1220 200	15.14 460.00 0.000515/0.00152	392.50 157.0	Geosteel G600 Geosteel G600 Geosteel G2000 Geosteel G2000 Geosteel G2000 Geosteel G2000	0.0149 0.0107 0.0080 0.0085 0.0070 0.0075
Bencardino and Condello [41]	A-EB B-EB	150 250/400 365	3000/4500 900/1500 100/150	16.70 367.1 0.000657	401.92 100.50	Kimisteel INOX	0.00587 0.00599
Ombres and Verre [43]	B-1L	140 300 269	4500 1600 70	19.4 474 0.00028	113.04 28.26	Geosteel G1200	0.0074

Table 9. Experimental database of bond tests on concrete prism.

Experimental Work	Specimen	F_{max} (kN)	$\sigma_{lim,conv}$ (MPa)	$\varepsilon_{lim,conv}$	$\varepsilon^{(\alpha)}{}_{lim,conv}$	Reinforcement Fibre
Matana et al. [45]	G-12-1 G-12-2 G-12-3	28.48 25.37 21.81	727.62 648.04 557.09	0.00364 0.00324 0.00279	0.00546 0.00486 0.00418	Hardwire 3SX
Realfonzo et al. [46]	30 LD-2 30 LD-3	14.30 15.73	1692.98 1858.74	0.00870 0.00955	0.01304 0.01432	Geosteel G600
	30 MD-1 30 MD-2 30 MD-3	16.64 16.01 17.66	655.28 630.47 695.45	0.00337 0.00324 0.00357	0.00505 0.00486 0.00536	Geosteel G2000
Bencardino and Condello [44]	200 S 250 S 300 400 S	7.24 7.20 6.17 7.90	603.33 600.00 514.17 658.33	0.00319 0.00317 0.00272 0.00348	0.00479 0.00476 0.00408 0.00522	Kimisteel INOX
Ascione et al. [47]	30LM-10-1-1 30LM-10-1-2 30LM-10-1-3	16.43 17.80 18.25	972.19 1053.25 1079.88	0.00499 0.00541 0.00555	0.00749 0.00811 0.00832	Geosteel G1200

Concerning the database of direct shear test (Table 9), the maximum load (F_{max}), the maximum stress (σ_{max}), and the intermediate debonding strain calculated with the CNR-DT 215/2018 procedure ($\varepsilon^{(\alpha)}{}_{lim,conv}$) were reported. The database was collected considering the specimens with enough bonded length (≥200 mm) in order to avoid results where the maximum debonding load is not reached. The results obtained from the debonding formula were collected in Table 11 for each set of experimentally tested beam. Finally, the comparison in terms of average values weas summarized in Table 12. $Diff_1$ is the percentual difference between the experimental debonding strain and the CNR-DT

215/2018 prediction, whereas $Diff_2$ represents the corresponding comparison between the experimental values and predictive formula.

Table 10. Properties of the steel fibres.

Steel Textile	E_{f1} (MPa)	E_{f2} (MPa)	E_{fm} (MPa)	t_f (mm)	f_{fu} (MPa)	ε_{fu}	Cord Area (mm^2)	Spacing (Cord/cm)	Density
Hardwire 3SX	200,000	200,000	200,000	0.382	1701.83	0.0168	0.813	4.70	M
Geosteel G600	206,000	183,400	194,700	0.086	3191.00	0.0219	0.538	1.57	L
Geosteel G1200	206,000	183,400	194,700	0.169	3138.30	0.0214	0.538	3.14	L-M
Geosteel G2000	206,000	183,400	194,700	0.254	3085.70	0.0209	0.538	4.72	H
Kimisteel INOX	189,000	189,000	189,000	0.240	1400.73	0.0148	0.470	5.20	H

Table 11. Debonding strains obtained from the predictive formula.

Ref.	ID	n_f	$\varepsilon_{f,deb}{}^{AV}$
Barton et al. [42]	SRG-2	1	0.0077
Napoli and Realfonzo [21]	SRG-1LD	1	0.0145
	SRG-2LD	2	0.0101
	SRG-1MD	1	0.0082
	SRG-1MD-A	1	0.0082
	SRG-1MD-B	1	0.0082
	SRG-2MD	2	0.0057
Bencardino and Condello [41]	B-EB	1	0.0086
Ombres and Verre [43]	B-1L	1	0.0115
	B-1L-1A	1	0.0115
	B-1L-2A	1	0.0115

Table 12. Experimental and theoretical comparisons.

Rif./Strengthening System	$\varepsilon_{f,max}{}^{AV}$	$\varepsilon_{lim,conv}{}^{AV}$	$\varepsilon^{(\alpha)}{}_{lim,conv}{}^{AV}$	$\varepsilon_{f,deb}{}^{AV}$	$Diff_1$ (%)	$Diff_2$ (%)	Density	α_{real}
Barton et al./Hardwire 3SX	0.00650	0.00322	0.00483	0.00655	−25.66	0.83	M	1.49
Napoli and Realfonzo/Geosteel G600	0.0128	0.00912	0.0137	0.0123	6.89	−3.72	L	1.40
Napoli and Realfonzo/Geosteel G2000	0.00780	0.00339	0.00509	0.00761	−34.35	−1.84	H	2.28
Bencardino and Condello/Kimisteel INOX	0.00599	0.00314	0.00471	0.00862	−21.30	43.87	H	1.91
Ombres and Verre/Geosteel G1200	0.00740	0.00532	0.00797	0.0102	7.77	37.83	L-M	1.39

The coefficient of transition between the two values (α_{real}) ranges from 1.5 (for low-density fibres) to about 2 (for fibres with increasing density). In fact, the experimental results show that both proposed methodologies lead to reliable results in the case of low-density and low/medium-density steel strip. The high surface density fibres are characterized by a premature debonding due to the difficult impregnation of the inorganic matrices, which makes it more difficult to predict the failure strain. The α value for high density fibres is due to a small end debonding strain. It can be generally concluded that the procedure proposed by the CNR-DT 215/2018 Guideline is conservative for the flexural strength of Steel-FRCM strengthened beams with dense fibres. Therefore, considering the characteristic values and dividing them by the partial factor, even lower values would be obtained.

On the other hand, the procedure proposed appears too general in indicating a single transition coefficient for all FRCM systems. In the marketplace, there are countless matrices with different mechanical properties. Moreover, the reinforcing fibres show different elastic modulus and tensile strength. Finally, the mass per unit of area, as demonstrated with the two steel fibres analysed, considerably changes the behaviour and the debonding strains. The predictive formulas are simple and easy to use and are determined only by the mechanical (E_f) and geometric (n_f and t_f) properties of the steel fibres (available from the technical datasheets). Future developments should focus on the proposal of the design formula of beams to develop more precise design guidelines, considering an extended database involving the other FRCM systems (Carbon and PBO).

6. Conclusions

The present paper investigated the behaviour of different Steel-FRCM systems bonded to concrete substrates. The total characterization of the materials was carried out by means of direct tensile tests on steel textiles, and compressive/flexural tests of the cementitious matrix. The theoretical calculations are based on two alternative procedures in order to identify the key parameter in the flexural strengthening of RC beams. The results were compared, producing an experimental database from the already published research. Based on the experimental results and theoretical data, the following conclusions can be drawn:

1. The bond properties of Steel-FRCM composites are strongly affected by the tensile strength and mass per unit area of the steel strips. The broad variability of the components (type of steel and matrices) produces different levels of performance. In particular, with reference to the efficiency factor σ_{max}/f_f, the best bond performance is obtained using low-density steel fibre (GLV). The efficiency factors are 34.18% and 93.73% for SS and GLV, respectively.
2. Different failure modes were observed from the experimental results. The debonding mainly occurs at the matrix–fibre interface (mode C) and between surface and Steel-FRCM composite (mode B), confirming the non-involvement of the concrete substrates. The failure mode of the galvanized fibre (GLV) is particularly positive, with the failure of the steel fibre outside the composite strip (without sliding).
3. The procedure reported in the CNR document provides information that may be calibrated in relation to the several materials available for the strengthening of structural elements. It seems reductive to indicate a single coefficient for all the types of FRCM reinforcement.
4. Specifically, high-density steel fibre reinforcement requires a transition coefficient around 2. The coefficient of 1.5 gives satisfactory results for low-density fibre. When the failure occurs due to the rupture of the reinforcement, as in the case of the GLV steel strip, the debonding phenomenon does not occur and the transition coefficient is equal to 1.
5. The predictive formulas provide an accurate prediction of the strain corresponding to debonding also through the calibration of a suitable safety coefficient. They can be transferred to engineers for design practice applications, owing to their simplicity.
6. The theoretical calculations were based on a database of experimental results collected from the scientific literature in order to investigate the intermediate debonding strain in the flexural strengthening applications. Based on the results, it is apparent that both procedures can be successfully used in the flexural strengthening design process, but specific suggestion should be investigated. High-mass density fibres show higher error ratios in predicting intermediate strains.

Despite studies on FRCM systems having achieved adequate knowledge in recent years, further steps must be taken, and the time is ripe for the final drafting of design documents to be transmitted to the professional world.

Author Contributions: Conceptualization, F.B. and M.N.; funding acquisition, F.B.; project administration, F.B.; methodology, F.B.; resources, F.B.; supervision, F.B.; validation, F.B.; visualization, F.B.; writing—review, F.B.; data curation, M.N.; investigation, M.N.; formal analysis, M.N.; writing—original draft preparation, M.N. All authors have read and agreed to the published version of the manuscript.

Funding: The financial support of the Italian Department of Civil Protection (ReLUIS—DPC Programme 2022–2024, WP14: Contributions for Standards regarding the use of Innovative Structural Materials for Sustainability of the Construction) are gratefully acknowledged. A special acknowledgment is also addressed to Kimia S.p.A. for providing their materials and technical support for the experimental test.

Institutional Review Board Statement: Not applicable.

Informed Consent Statement: Not applicable.

Data Availability Statement: Not applicable.

Conflicts of Interest: The authors declare no conflict of interest.

References

1. Papanicolaou, C.G.; Triantafillou, T.C.; Karlos, K.; Papathanasiou, M. Textile reinforced mortar (TRM) versus FRP as strengthening material of URM walls: In plane cyclic loading. *Mater. Struct.* **2007**, *40*, 1081–1097. [CrossRef]
2. Fuseini, M.; Yousry Zaghloul, M.M.; Elkady, M.F.; El-Shazly, A.H. Evaluation of synthesized polyaniline nanofibres as corrosion protection film coating on copper substrate by electrophoretic deposition. *J. Mater. Sci.* **2022**, *57*, 6085–6101. [CrossRef]
3. Yousry Zaghloul, M.M.; Yousry Zaghloul, M.M.; Yousry Zaghloul, M.M. Developments in polyester composite materials—An in-depth review on natural fibres and nano fillers. *Compos. Struct.* **2021**, *278*, 114698. [CrossRef]
4. Yousry Zaghloul, M.M.; Yousry Zaghloul, M.M. Influence of flame retardant magnesium hydroxide on the mechanical properties of high density polyethylene composites. *J. Reinf. Plast. Compos.* **2017**, *36*, 1802–1816. [CrossRef]
5. Ascione, G.L.; de Felice, S.; De Santis, A. qualification method for externally bonded Fibre Reinforced Cementitious Matrix (FRCM) strengthening systems. *Compos. B Eng.* **2015**, *78*, 497–506. [CrossRef]
6. *AC434*; Proposed Acceptance Criteria for Masonry and Concrete Strengthening Using Fiber-Reinforced Cementitious Matrix (FRCM) Composite Systems. ICC-Evaluation Service: Whittier, CA, USA, 2013.
7. De Santis, S.; de Felice, G. Tensile behaviour of mortar-based composites for externally bonded reinforcement systems. *Compos. B Eng.* **2015**, *68*, 401–413. [CrossRef]
8. De Santis, S.; de Felice, G. Tensile behaviour and durability of mortar-based strengthening systems with glass-aramid textile. *J. Key Eng. Mater.* **2015**, *624*, 346–353. [CrossRef]
9. Ombres, L.; Verre, S. Experimental and Numerical Investigation on the Steel Reinforced Grout (SRG) Composite-to-Concrete Bond. *J. Compos. Sci.* **2020**, *4*, 182. [CrossRef]
10. Bencardino, F.; Nisticò, M.; Verre, S. Fibers, Experimental Investigation and Numerical Analysis of Bond Behavior in SRG-Strengthened Masonry Prisms Using UHTSS and Stainless-Steel. *Fibers* **2020**, *8*, 8. [CrossRef]
11. Younis, A.; Ebead, U. Bond characteristics of different FRCM systems. *Constr. Build. Mater.* **2018**, *175*, 610–620. [CrossRef]
12. Hadad, H.A.; Erickson, B.; Nanni, A. Flexural analysis and design of FRCM-strengthened RC beams. *Constr. Build. Mater.* **2020**, *244*, 118371. [CrossRef]
13. Marcinczak, D.; Trapko, T.; Musiał, M. Shear strengthening of reinforced concrete beams with PBO-FRCM composites with anchorage. *Compos. B Eng.* **2019**, *158*, 149–161. [CrossRef]
14. Feng, R.; Liu, Y.; Zhu, J.-H.; Xing, F. Flexural behaviour of C-FRCM strengthened corroded RC continuous beams. *Compos. Struct.* **2020**, *245*, 112200. [CrossRef]
15. Loreto, G.; Babaeidarabad, S.; Leardini, L.; Nanni, A. RC beams shear-strengthened with fabric-reinforced-cementitious-matrix (FRCM) composite. *Inter. J. Adv. Struct. Eng. (IJASE)* **2015**, *7*, 341–352. [CrossRef]
16. Salsavilca, J.; Yacila, J.; Tarque, N.; Camata, G. Experimental and analytical bond behaviour of masonry strengthened with steel reinforced grout (SRG). *Constr. Build. Mater.* **2020**, *238*, 117635. [CrossRef]
17. Larrinaga, P.; Garmendia, L.; Piñero, I.; San-José, J.T. Flexural strengthening of low-grade reinforced concrete beams with compatible composite material: Steel Reinforced Grout (SRG). *Constr. Build. Mater.* **2020**, *235*, 117790. [CrossRef]
18. Yacila, J.; Salsavilca, J.; Tarque, N.; Camata, G. Experimental assessment of confined masonry walls retrofitted with SRG under lateral cyclic loads. *Eng. Struct.* **2019**, *199*, 109555. [CrossRef]
19. Wakjira, T.G.; Ebead, U. Experimental and analytical study on strengthening of reinforced concrete T-beams in shear using steel reinforced grout (SRG). *Compos. B Eng.* **2019**, *177*, 107368. [CrossRef]
20. Papanikolaou, G.E.T.V.K.; Lioupis, C.; Hajirasouliha, I. Steel-Reinforced Grout (SRG) strengthening of shear-critical RC beams. *Constr. Build. Mater.* **2019**, *216*, 68–83.
21. Napoli, A.; Realfonzo, R. Reinforced concrete beams strengthened with SRP/SRG systems: Experimental investigation. *Constr. Build. Mater.* **2015**, *93*, 654–677. [CrossRef]
22. Aiello, M.A.; Bencardino, F.; Cascardi, A.; Realfonzo, R.; Verre, S. Masonry columns confined with fabric reinforced cementitious matrix (FRCM) systems: A round robin test. *Constr. Build. Mater.* **2021**, *298*, 123816. [CrossRef]
23. *ACI 549.4R-20*; Guide to Design and Construction of Externally Bonded Fabric-Reinforced and Steel-Reinforced Grout Systems for Repair and Strengthening of Concrete Structures. American Concrete Institute: Farmington Hills, MI, USA, 2013.

24. National Research Council (CNR). *Guide for the Design and Construction of Externally Bonded Fibre Reinforced Inorganic Matrix Systems for Strengthening Existing Structures; CNR-DT 215/2018 (updated version 30 June 2020)*; CNR: Rome, Italy, 2020; Available online: https://www.cnr.it/en/node/12827 (accessed on 17 June 2022).
25. Bencardino, F.; Carloni, C.; Condello, A.; Focacci, F.; Napoli, A.; Realfonzo, R. Flexural behaviour of RC members strengthened with FRCM: State-of-the-art and predictive formulas. *Compos. B Eng.* **2018**, *148*, 132–148. [CrossRef]
26. ST3-0221. Kimia S.p.A. Available online: www.kimia.it (accessed on 10 January 2020).
27. ST7-0221. Kimia S.p.A. Available online: www.kimia.it (accessed on 10 January 2020).
28. ST6-0319. Kimia S.p.A. Available online: www.kimia.it (accessed on 10 January 2020).
29. *EN 1504-3:2005*; Products and Systems for the Protection and Repair of Concrete Structures—Definitions, Requirements, Quality Control and Evaluation of Conformity—Part 3: Structural and non-Structural Repair. 2005. Available online: https://standards.iteh.ai/catalog/standards/cen/901c7ca2-4f42-4478-a8e1-7e56ee6a8475/pren-1504-3-rev (accessed on 17 June 2022).
30. *EN 1504-4:2004*; Products and Systems for the Protection and Repair of Concrete Structures—Definitions, Requirements, Quality Control and Evaluation of Conformity—Part 4: Structural Bonding. Available online: https://standards.iteh.ai/catalog/standards/cen/ab0b5079-46c0-49ed-80ee-48254718963f/en-1504-4-2004 (accessed on 17 June 2022).
31. *EN 12190:1998*; Product and System for the Protection and Repair Concrete Structures—Test Methods—Determination of Compressive Strength of Repair Mortar. Available online: https://standards.iteh.ai/catalog/standards/cen/4191a705-4001-4412-ae57-f21e7994bb79/en-12190-1998 (accessed on 17 June 2022).
32. *EN 1015-11:2019*; Methods of Test for Masonry Units—Part 11: Of flexural and Compressive Strength of Hardened Mortar. Available online: https://standards.iteh.ai/catalog/standards/cen/14596d4c-119b-4a78-94e1-3fe481a29bde/en-1015-11-2019 (accessed on 17 June 2022).
33. D'Antino, T.; Colombi, P.; Carloni, C.; Sneed, L.H. Estimation of a matrix-fiber interface cohesive material law in FRCM-concrete joints. *Compos. Struct.* **2018**, *193*, 103–112. [CrossRef]
34. Razavizadeh, A.; Ghiassi, B.; Oliveira, D.V. Bond behavior of SRG-strengthened masonry units: Testing and numerical modeling. *Constr. Build. Mater.* **2014**, *64*, 387–397. [CrossRef]
35. Bellini, A.; Aiello, M.A.; Bencardino, F.; Bello, C.B.D.C.; Castori, G.; Cecchi, A.; Ceroni, F.; Corradi, M.; D'Antino, T.; De Santis, S.; et al. Influence of different set-up parameters on the bond behavior of FRCM composites. *Constr. Build. Mater.* **2021**, *308*, 124964. [CrossRef]
36. Cheng, J.F.; Teng, J.G. Anchorage strength models for FRP and steel plates bonded to concrete. *J. Struct. Eng. ASCE* **2001**, *127*, 784–791. [CrossRef]
37. Mazzotti, C.; Savoia, M.; Ferracuti, B. A new single-shear set-up for stable debonding of FRP-concrete joints. *Constr. Build. Mater.* **2009**, *23*, 1529–1537. [CrossRef]
38. De Felice, G.; Aiello, M.A.; Caggegi, C.; Ceroni, F.; de Santis, S.; Garbin, E.; Gattesco, N.; Hojdys, Ł.; Krajewski, P.; Kwiecien, A.; et al. Recommendation of RILEM TC 250-CSM: Test method for Textile Reinforced Mortar to substrate bond characterization. *Mater. Struct.* **2018**, *51*, 95. [CrossRef]
39. *EN 1990:2002*; Eurocode 0: Basis of Structural Design. CEN—European Committee for Standardization: Brussels, Belgium, 2002. Available online: https://standards.iteh.ai/catalog/standards/cen/be4b05f7-4c56-4e2e-a88d-56fce873fcbc/en-1990-20022002 (accessed on 17 June 2022).
40. Bencardino, F.; Nisticò, M. Predictive Strain Debonding in RC Beams Externally Strengthened with S-FRCM. In Durability and Sustainability of Concrete Structures (DSCS-2018). In Proceedings of the 2nd International Workshop, Moscow, Russia, 6–7 June 2018.
41. Bencardino, F.; Condello, A. Innovative solution to retrofit RC members: Inhibiting-Repairing-Strengthening (IRS). *Constr. Build. Mater.* **2016**, *117*, 171–181. [CrossRef]
42. Barton, B.; Wobbe, E.; Dharani, L.R.; Silva, P.; Birman, V.; Nanni, A.; Alkhrdaji, T.; Thomas, J.; Tunis, G. Characterization of reinforced concrete beams strengthened by steel reinforced polymer and grout (SRP and SRG) composites. *Mater. Sci. Eng. A* **2005**, *412*, 129–136. [CrossRef]
43. Ombres, L.; Verre, S. Flexural Strengthening of RC Beams with Steel-Reinforced Grout: Experimental and Numerical Investigation. *J. Compos. Constr. ASCE* **2019**, *23*, 04019035. [CrossRef]
44. Bencardino, F.; Condello, A.; Ashour, A.F. Single-lap shear bond tests on Steel Reinforced Geopolymeric Matrix-concrete joints. *Compos. B Eng.* **2017**, *110*, 62–71. [CrossRef]
45. Matana, M.; Nanni, A.; Dharani, L.; Silva, P.; Tunis, G. Bond performance of steel reinforced polymer and steel reinforced grout. In Proceedings of the International Symposium on Bond Behaviour of FRP in Structures (BBFS 2005), Hong Kong, China, 7–9 December 2005.
46. Realfonzo, R.; Napoli, A.; Ascione, F.; Lamberti, M. Bond behavior of SRP/SRG systems on concrete substrate: Experimental investigations. In Proceedings of the 4th Workshop on the New Boundaries of Structural Concrete, Anacapri, Italy, 29 September–1 October 2016.
47. Ascione, F.; Lamberti, M.; Napoli, A.; Realfonzo, R. Experimental bond behavior of Steel Reinforced Grout systems for strengthening concrete elements. *Constr. Build. Mater.* **2020**, *232*, 117105. [CrossRef]